Journal of Advanced Zoology

ISSN: 0253-7214

Volume ***44*** *Issue* ***03 Year 2023*** *Page* ***291:308***

Hybrid Optimal Deep Learning with IoT Based Smart Based Monitoring and Maintenance System for Axial Flow Fan using Feature Optimization

Mădălin Andreica[1*], Alexandra Offenberg[2]

[1]*Department of Mechanical, Industrial and Transportation Engineering, University of Petroșani, Romania.*
[2]*Department of Mechanical, Industrial and Transportation Engineering, University of Petroșani Romania.*
Email: Alexandra.offenberg@yahoo.ro
**Corresponding author's E-mail: mady_andreica@gmail.com*

Article History

Received: 06 June 2023
Revised: 25 Sept 2023
Accepted:06 Oct 2023

Abstract

Axial flow fan is a mechanical fan that generates airflow in the same direction as its rotational axis. These fans find widespread use in various applications, including ventilation, cooling, and air circulation across industrial, commercial, and residential settings. However, designing these fans can be challenging in the fan manufacturing industry due to the need to accommodate diverse operating conditions. This complexity arises from the fact that multiple design parameters significantly influence fan performance, requiring careful consideration and optimization to ensure efficient operation across various scenarios. In this paper, we present a technique for monitoring and maintenance of axial flow fans using hybrid optimal deep learning with IoT system. Our method leverages the pre-trained U-Net architecture to extract hidden features effectively from the dataset. Furthermore, we introduce an improved triple tree-seed optimization (IT2SO) algorithm for feature optimization, which identifies the most optimal features among the extracted ones. To make informed decisions about axial flow fan process monitoring, we propose the deep boosted hybrid learning (DBHL) technique as the decision model to maintain the proper operation. To validate the effectiveness of proposed IT2SO+DBHL technique, we have conducted experiments using the air movement and control association international (AMCA) dataset. The results demonstrate the superior performance of our monitoring approach compared to existing techniques across various evaluation measures.

Keywords: A*xial flow fan, Feature extraction, Feature optimization, Process monitoring, Fan manufacturing*

1. Introduction

The fan manufacturing industry [1] encompasses the production of various types of fans designed for diverse applications, including cooling, ventilation, exhaust, and more. One common type of fan within this industry is the axial flow fan, also known as a propeller fan. Axial flow fans [2][3] move air or gas parallel to their axis of rotation, with blades resembling aircraft or boat propellers. They are highly efficient at generating a large volume of airflow at relatively low pressure, making them suitable for cooling electronic equipment, providing building ventilation, and cooling radiators in vehicles. These fans vary in size from small desktop versions to massive industrial ones used in power plants [4]. Depending on their design and speed, they can produce varying levels of noise, with quieter versions used in noise-sensitive environments. Axial flow fans come in different types, such as tube-axial fans, vane-axial fans, and propeller fans, catering to specific airflow requirements and industry needs [5]. Overall, the fan manufacturing industry plays a pivotal role in providing air movement and ventilation solutions across a wide range of sectors.

A monitoring and maintenance system for axial flow fans comprises a comprehensive set of practices and tools designed to ensure the dependable and efficient operation of these fans while promptly identifying and addressing potential issues or failures [6]. This system is vital for a wide range of

applications utilizing axial flow fans, including industrial facilities, HVAC systems, and power plants [7]. The system typically includes routine visual inspections to detect visible signs of wear and damage on fan components, such as blades, motors, and housings. Additionally, vibration sensors are often employed to monitor fan vibrations, with unusual or excessive vibrations serving as indicators of mechanical problems, imbalances or misalignments [8]. Temperature sensors may also be in use to keep tabs on motor and bearing temperatures, with elevated temperatures signaling potential issues like overheating or insufficient lubrication. Monitoring airflow and noise levels are other essential aspects of this system, helping identify performance deviations or abnormal noise that could hint at underlying fan problems [9]. Condition-based maintenance strategies are a crucial element, leveraging data from sensors and inspections to schedule maintenance based on the actual condition of the fan rather than predetermined time intervals, thus optimizing maintenance efficiency. Bearing-equipped fans require a well-maintained lubrication schedule to prevent bearing failure and fan malfunctions. Regular cleaning of fan blades and surrounding areas is also fundamental to prevent dirt and debris buildup, which can reduce efficiency and increase wear [10].

Alignment and balancing checks are performed periodically to ensure that the fan operates correctly, preventing issues like misalignment or imbalance that may lead to excessive wear and vibrations. Data from monitoring sensors is logged and analyzed over time, enabling the detection of trends or patterns indicative of impending problems. Some systems may also utilize advanced predictive maintenance techniques to forecast maintenance needs. Additionally, protocols for emergency shutdown procedures are established to safely halt fan operation in the event of critical failures or emergencies, safeguarding against further damage or risks to personnel. Overall, the design a monitoring and maintenance system for axial flow fans ensures equipment longevity, minimal downtime, enhanced energy efficiency, and improved operational reliability, tailored to the specific needs and importance of the fan within its application [11][12].

Deep learning [13]-[20] can play a significant role in enhancing the monitoring and maintenance system for axial flow fans. The deep neural networks (DNNs) [13] or convolutional neural networks (CNNs) [14] can be trained on historical data from the axial flow fan's operation. These models can learn to recognize normal operating patterns and detect anomalies in real-time. Unusual vibrations, temperature spikes, or airflow deviations that may not be immediately apparent to human operators can be flagged by the deep learning system, triggering maintenance alerts [15]. Deep learning models can forecast the remaining useful life of critical components, such as fan blades or bearings. By analyzing historical data and patterns of wear and tear, these models can provide maintenance schedules that are more precise and cost-effective [16]. This approach helps avoid both premature maintenances which can costly and unplanned downtime due to component failures. Deep learning models can be integrated with the internet of things (IoT) sensors on the fan and surrounding equipment [17]-[19]. These models can process the data generated by these sensors in real-time, allowing for more precise monitoring and quicker response to potential issues. Deep reinforcement learning [20] can used to optimize the operation of axial flow fans for energy efficiency. The system can learn to adjust fan speed and other parameters in response to changing environmental conditions, thereby reducing energy consumption while maintaining adequate ventilation or cooling.

Our contributions. To enhance the fan manufacturing industry and address the complexity of design parameters, we present a novel hybrid optimal deep learning-based monitoring and maintenance system for efficient monitoring of axial flow fan operations. This system makes significant contributions to the field, which can be summarized as follows: Our work focuses on the development of a hybrid optimal deep learning-based monitoring system for axial flow fans, providing an effective solution to tackle the challenges posed by intricate design parameters.

1. We employ the U-Net pre-trained architecture to enhance feature extraction, allowing us to uncover hidden features within the dataset more effectively.
2. To optimize the extracted features, we introduce an improved algorithm called the triple tree-seed optimization (IT2SO) algorithm. This algorithm meticulously analyzes the features and selects the most optimal ones for further processing.

3. For the decision-making aspect of axial flow fan process monitoring and maintenance, we propose the utilization of the Deep Boosted Hybrid Learning (DBHL) technique. This decision model enhances the overall monitoring process.

The structure for the rest of this paper is outlined as follows: Section 2 describes the review of literature on the axial flow fan design and process monitoring. Section 3 gives the detailed working process of proposed technique. The results and comparative analysis of proposed and existing techniques have discussed in Section 4. Finally, Section 5 concludes the research work.

Related work

In this section, we present the literature review on the design of axial flow fan with the deep learning-based monitoring and maintenance system.

State of art study

Mesalhy et al. [21] developed a computational fluid dynamics (CFD) model that focused on heat transfer and airflow across finned surfaces. They correlated fan pressure jump with the volumetric flow rate of a high-speed SUNON fan, considering different rotational speeds and ambient pressures measured in a fan loop. To validate their CFD predictions, they constructed a test setup consisting of a finned surface attached to a heated cylindrical aluminum block, connected to a fan. Comparing predicted values to measured results, they reduced the average temperature difference ($T-T\infty$) discrepancy from 1.6°C using the k-ε Realizable model to 0.31°C with the k-ω SST model. They also conducted numerical simulations to evaluate the impact of fin shape, quantity, and thickness on fin structure cooling effectiveness, finding that straight plate fins outperformed offset-strip and corrugated designs.

Angelini et al. [22] conducted initial research to explore correlations between design parameters and performance in axial flow fans using a database of approximately 4000 individual cases. They aimed to demonstrate the methodology's applicability to incomplete datasets typical in fan manufacturers' records. They employed statistical techniques like principal component analysis (PCA) and projection to latent structures (PLS) in designing and optimizing industrial turbo machinery. Within the database, they fully characterized each individual's geometry, deriving parameters such as blade chord and twist distributions, hub pitch angles, and 2D blade profiles at various radii.

Li et al. [23] developed and optimized a high-loaded transonic fan stage with a curvature control technique. Through 3D optimizations, they achieved a fan stage with a total pressure ratio of 2.49 and an adiabatic efficiency exceeding 87% at the design operating point. The geometric curvature of the blade passage significantly influenced airflow and boundary layer behavior. Their optimization strategy minimized secondary flow losses and expanded the fan stage's stall margin. This approach offered high precision, operational flexibility, and rapid design iteration for enhancing high-loaded fan and compressor capabilities and advancing design system development.

Shahsavari et al. [24] introduced an innovative approach to redesigning an axial flow fan, aiming to maintain constant diffusion and achieve radial equilibrium. They developed a computer program to extract three-dimensional fan geometry and estimate parameter distributions along the fan's span. Computational fluid dynamics (CFD) tools were used to analyze the redesigned fan's performance under various operating conditions, including the design point and off-design scenarios. Comprehensive analysis showed advantages over NASA Rotor 67, including a higher total pressure ratio, desired pressure ratio at lower rotational speeds, higher efficiency, greater bypass air within a constant diameter, and reduced fuel consumption while generating the same specific thrust force.

Zhen-yu et al. [25] introduced a method for early fault assessment to predict the operational trajectory of a low-speed axial fan (LAF). Their approach combined vibration-electric data fusion, support vector machine (SVM) with particle swarm optimization (PSO), and cross-validation (CV) to anticipate the LAF's operational states. Vibration signals, adversely affected by the fan housing, were complemented by electric parameters, which offered advantages in terms of ease of acquisition, precision, resistance to interference, and rich operational information. To validate their approach, an experimental study established an operational state model for the LAF by fusing vibration and electric data.

Kumar et al. [26] analyzed pressure data using windowed Fourier analysis to distinguish operational regions as a fan transitioned from its operational state to stall. They identified four statistical parameters to effectively describe pressure data and reduce complexity. Applying K-means clustering to these parameters enabled automated differentiation of operational regions. Both types of analyses consistently identified a transitional region between no activity and stall, characterized by intermittent parameter variations and fluctuating Fourier frequencies.

Ciaburro et al. [27] automated fan maintenance procedures using acoustic emission data and deep learning techniques to diagnose faults. Their study focused on detecting dust deposits on axial fan blades. They employed a pre-trained neural network called SqueezeNet, originally designed for ImageNet, to analyze spectrograms extracted from acoustic emission recordings of the fan in both "No-Fault" and "Fault" conditions. Transfer learning on these spectrogram images resulted in a promising accuracy rate of 0.95.

Liang et al. [28] introduced an innovative concept inspired by the forked caudal fin of fish, modifying the trailing edge of a prototype fan. Comprehensive experiments explored the impact of this bionic forked trailing-edge design on aerodynamic and aeroacoustic performance. Results indicated significant advantages, including altered blade loading distribution, reduced pressure disparity near the trailing edge, and reduced discrete noise, particularly at the blade passing frequency (BPF) and its harmonics. The optimal bionic forked trailing-edge structure achieved a maximum power-saving rate of 7.5% and reduced aerodynamic noise by 0.3 to 0.8 dB with a specific included angle of 13.5°.

Ding et al. [29] introduced a blade design methodology using standard-form rational quadratic Bezier curves to define blade angles and bending angles. They employed the Dendrite Net neural network model to predict fan pneumatic performance and applied a non-dominated sorting genetic algorithm for global optimization. The optimized blade load distribution exhibited radial uniformity and reduced adverse effects of suction surface separation vortex and passage vortex. Experiments validated their methodology, resulting in a significant increase in fan performance, with a maximum efficiency increase of 5.44% and a 2.47% increase in maximum total pressure coefficient.

Chen et al. [30] analyzed the relationship between airflow volume rate and geometric parameters of guide vanes in a selected axial fan. They used design of experiments (DOE) and computational fluid dynamics (CFD) techniques, identifying optimal parameters using the Gaussian Process method. The study highlighted that the number of guide vanes and the total chord of these vanes had nonlinear impacts on airflow volume rate, with vane chord emerging as the primary influencing factor in their specific configuration. Optimal guide vane design suggested that reducing vane chord by 38 mm and increasing the number of vanes to 18 could result in greater airflow volume at the same rotational speed.

Summary of Research gaps

A monitoring and maintenance system for axial flow fans is crucial for several reasons. First and foremost, it ensures the reliability and safety of these fans, which are commonly employed in critical applications such as ventilation, cooling systems, and industrial processes. Detecting issues early through monitoring prevents potential failures that could lead to accidents or costly downtime. Moreover, energy efficiency is paramount, and efficient fan operation is essential for conserving energy. Regular monitoring allows for adjustments and maintenance to keep the fan running at peak efficiency, ultimately reducing energy consumption and associated costs. Proper maintenance practices ensure that axial flow fans last longer, reducing the need for frequent replacements. This, in turn, leads to cost savings and minimizes the environmental impact associated with manufacturing and disposing of fans. Cost reduction is another advantage, as scheduled maintenance based on actual equipment condition is more cost-effective than reactive maintenance, which tends to be more expensive and disruptive. With a monitoring system, maintenance needs are identified in advance, mitigating unexpected repair costs. Furthermore, a monitoring and maintenance system helps optimize fan performance, aligning it with changing environmental conditions. Monitoring systems play a critical role in ensuring that fans meet emission standards and environmental requirements [21][22]. Moreover, these systems help reduce unplanned downtime due to fan failures, which can result in production losses and missed deadlines. Additionally, data-driven decision-making is used by monitoring systems, providing valuable insights into fan performance and condition [23]. This data enables informed decisions regarding maintenance

schedules, upgrades, or replacements. In industrial settings, proper fan functioning is often essential for safety compliance. Monitoring systems ensure that fans are in compliance with safety regulations and standards, contributing to a safer working environment.

The design of axial flow fans comes with set of intricate challenges that engineers and designers must navigate. One paramount concern is achieving high efficiency while minimizing energy losses attributed to factors, aerodynamic inefficiencies, friction, and internal turbulence within the fan structure [24]. Simultaneously, managing noise production is crucial, particularly in applications where noise reduction is a primary consideration, demanding the design of fans that operate quietly while maintaining peak performance [25]. Aerodynamic performance is another vital aspect, requiring the optimization of blade shapes, angles, and curvature to attain desired characteristics such as high airflow rates and pressure rises [26]. In certain applications involving the use of axial flow fans with liquids, the risk of cavitations, phenomenon where local pressure drops below the fluid's vapor pressure needs to be addressed through design considerations. Selecting appropriate materials for fan components is imperative, especially in environments with corrosive or high-temperature conditions, as material choices directly impact durability and maintenance needs [27]-[29]. Vibration is another challenge, as axial flow fans can experience vibration issues leading to noise and reduced lifespan. To mitigate these issues, proper balancing of fan features is essential [30].

2. Materials And Methods

This The conceptual structure of the proposed axial flow fan design, incorporating a deep learning-based monitoring and maintenance system, is illustrated in Fig. 1. This comprehensive process comprises several essential steps. Initially, data relevant to the axial flow fan's operation and performance is collected, typically sourced from the Air Movement and Control Association (AMCA) dataset, a valuable repository of fan-related information. Subsequently, the gathered data undergoes meticulous preprocessing to ensure its quality and suitability for analysis, which may involve cleaning, filtering, and formatting to eliminate noise or inconsistencies. Following data preprocessing, the key features pertinent to the axial flow fan are defined and selected for analysis. These features encompass crucial parameters such as chord length at the root and tip of the fan blades, pitch angle, twist angle, impeller diameter, hub outer diameter, blade number, tip clearance, and frame thickness. These features furnish vital insights into the fan's geometry and operational conditions. Deep feature extraction comes next, employing a U-Net architecture—a neural network framework commonly employed for image processing and segmentation tasks. In this context, it plays a pivotal role in extracting meaningful and relevant features from the fan data, thereby facilitating subsequent analysis and modeling. The extracted features then undergo optimization using the IT2SO algorithm. This optimization phase aims to enhance the quality and utility of the extracted features, rendering them more suitable for modeling and analysis purposes.

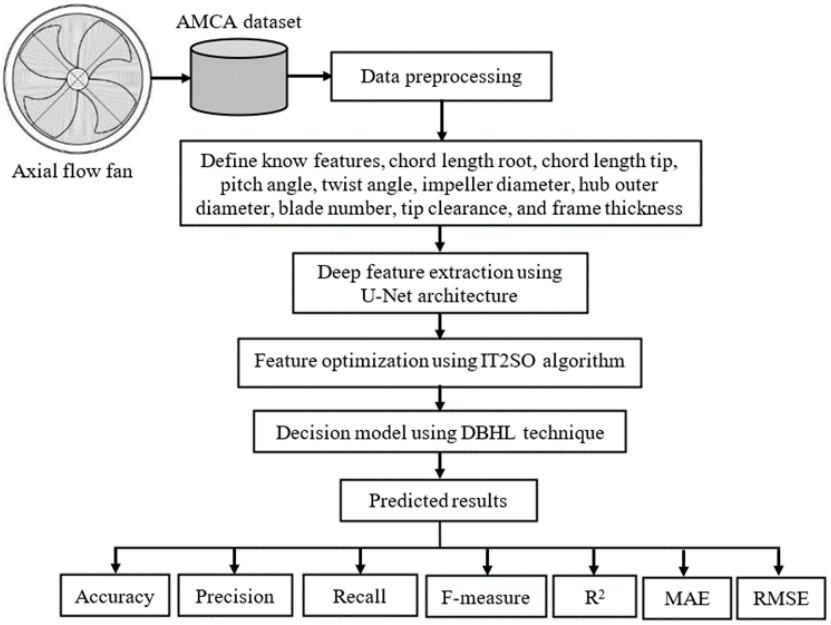

Fig. **1** Conceptual structure of proposed axial flow fan design using deep learning-based monitoring and maintenance

The core of the proposed system is the development of a decision model, achieved through the utilization of DBHL technique. This model incorporates the optimized features and is engineered to make predictions and assessments pertaining to the axial flow fan's performance and maintenance requisites. Lastly, the predicted results generated by the decision model undergo thorough evaluation. This evaluation encompasses array of performance metrics, encompassing accuracy, precision, recall, F-measure, R-squared (R2), mean absolute error (MAE), and root mean absolute squared error (RMASE). These metrics furnish valuable insights into the accuracy and reliability of the model in making predictions and assessments related to the monitoring and maintenance of the axial flow fan.

Deep feature extraction

Deep feature extraction is crucial step in our methodology harnesses the power of a pre-trained U-Net architecture to efficiently extract hidden and meaningful features from the dataset. The U-Net architecture is a convolutional neural network (CNN) framework initially designed for image segmentation tasks, but it has proven to be versatile in various applications. The U-Net architecture derives its name from its U-shaped structure, characterized by a contracting path (left side) followed by an expansive path (right side). The working process of U-Net using the deep feature extraction is given as follows.

- Contracting path: This initial phase of the U-Net captures and encodes information from the input data. It consists of series of convolutional and pooling layers that progressively reduce the spatial dimensions of the data while increasing the depth. This process extracts hierarchical features, starting with low-level details and gradually capturing more abstract and complex patterns.
- Bottleneck: The contracting path culminates in a bottleneck layer, which serves as a bottleneck for information flow. It retains essential features while discarding less relevant information, enhancing the network's focus on critical aspects of the data.
- Expansive path: The expansive path is the counterpart to the contracting path. It involves a series of up sampling and convolutional layers that gradually reconstruct the spatial dimensions of the data. This path's purpose is to decode the learned features and generate a segmentation map or, in our case, extract meaningful features.
- Skip connection: U-Net incorporates skip connections, which connect layers in the contracting path with corresponding layers in the expansive path. These connections allow the network to

retain fine-grained details during the up-sampling process, aiding in feature extraction and maintaining contextual information.

- Final feature map: At the end of the expansive path, the U-Net architecture produces a final feature map. This map contains the extracted features, which have been transformed and abstracted through the network's encoding and decoding process.

The pre-trained U-Net architecture offers a distinct advantage in feature extraction due to its ability to capture hierarchical and context-rich information from the dataset. By utilizing this architecture, our method ensures that the features extracted are not only effective but also well-suited for subsequent analysis and modeling tasks, contributing to the overall success of the monitoring and maintenance system for axial flow fans.

Feature Optimization

In the work, feature optimization following feature extraction involves refining and enhancing the extracted features to ensure they are highly informative and well-suited for the specific goals of monitoring and maintaining these fans. After extracting features from the dataset, they may contain redundant or noisy information. Feature optimization includes techniques to identify and remove redundant features and reduce noise, resulting in a cleaner and more meaningful feature set. In cases where the feature space is high-dimensional, dimensionality reduction techniques may be applied to reduce the number of features while retaining essential information. This can improve computational efficiency and prevent overfitting in subsequent modeling. Feature optimization involves normalizing or scaling features to ensure they are on a consistent scale and have standardized distributions, making them more suitable for modeling. Feature optimization involves selecting the most relevant features that have a significant impact on the monitoring and maintenance goals. By focusing on the most informative features, the subsequent modeling process becomes more efficient and effective.

We develop an improved Triple Tree-Seed Optimization (IT2SO) algorithm for feature optimization to identify the most optimal features from extracted ones. IT2SO builds upon the Tree-Seed Algorithm (TSA), which leverages tree-seed relationships for optimization [32]. TSA offers simplicity and robust solution exploitation, excelling in local search but facing limitations in global search. IT2SO enhances seed population initialization, vital for optimal solutions. The optimization involves four phases, starting with tree initialization.

$$t_{h,g} = l_{g,Min} + R_{h,g} \times \left(I_{g,Max} - l_{g,Max}\right) \quad (1)$$

where $l_{g,Min}$ represents the lower bound of the search space, $I_{g,Max}$ represents upper bound, and $R_{h,g}$ is assigned as a random value within the range [0, 1] for each dimension and location. Seed generation is achieved through

$$s_{h,g} = t_{h,g} + \alpha_{h,g} \times \left(N_g - t_{R,g}\right) \quad (2)$$

$$s_{h,g} = t_{h,g} + \alpha_{h,g} \times \left(t_{h,g} - t_{R,g}\right) \quad (3)$$

Here, $s_{h,g}$ represents the h-th seed in the g-th dimension produced by the h-th tree, and $t_{h,g}$ is the h-th tree in the same dimension. N_g represents the best tree location obtained thus far in the g-th dimension, and $t_{R,g}$ is a randomly selected tree from the g-th dimension's population. α is a scaling factor randomly generated within the range of [−1, 1], and 'h' and 'R' are different tree indices being updated. If the seeds' fitness values are better than the initial trees, the trees are updated, leading to a new optimal position. This process iterates through the three phases, eventually converging to the best value as the number of evaluations reaches its maximum. The termination condition is determined by the maximum number of function evaluations $Max\ fes$, which is computed and updated as follows:

$$Max\ fes = C \times 10{,}000 \quad (4)$$

$$fes = fes + ns \quad (5)$$

In IT2SO, 'ns' represents the number of seeds generated by a tree. The algorithm creates initial random candidate solutions and steers them toward the optimal solution using mathematical models based on sine and cosine functions. It employs random and adaptive variables to balance exploration and exploitation throughout various optimization stages. The position is updated in both phases as follows:

$$P_h^{T+1} = P_h^T + R_1 \times \sin(R_2) \times \left| R_3 X_h^T - P_h^T \right|, R_4 < 0.5 \quad (6)$$

$$P_h^{T+1} = P_h^T + R_1 \times \cos(R_2) \times \left| R_3 X_h^T - P_h^T \right|, R_4 \geq 0.5 \quad (7)$$

where P_h^T represents the current solution's position in the h-*t*h dimension at T-*t*h iteration, and X_h^T is the destination point's position in the same dimension. Random values R_1 , R_2 , R_3 , and R_4 in the range [0, 1] are used in the computation. SCA involves four main parameters: the h-*t*h dimension, R_1 , R_2 , R_3 , and R_4. R_1 determines the next position area, R_2 indicates the movement's distance to the target or outward, R_3 introduces randomness to the destination weight, either emphasizing ($R_3 > 1$) or deemphasizing ($R_3 < 1$) its effect. θ represents a uniform switching between sine and cosine functions. To balance exploration and exploitation, the range of sine and cosine functions adapts dynamically.

$$R_1 = m - s\frac{m}{t} \quad (8)$$

In the optimization process, T represents the current iteration, t is the maximum number of iterations, and m is a constant. In basic TTSA, the current best tree serves as the candidate tree, which can lead to local optima. SCA excels in global search capability, and it inspired a sine-random-distribution migration mechanism. IT2SO adopts a similar mechanism to tree migration. During tree migration, if the minimum of all seed values (ns(h)) is less than the objective value of the h-th tree, the original IT2SO is applied. Otherwise, new rules are implemented, where the first three trees in the current iteration become candidate components, and a sine function inspired by IT2SO is introduced to enhance diversity. These enhancements include the addition of two tree migration equations in this phase."

$$t_{h,g} = \left(t_{xn,1} + t_{xn,2} + t_{xn,3}\right)/3 + \left(N_g - t_{R,g}\right) * \sin\left(2 * xh * Rand\right) \quad (9)$$

$$t_{h,g} = \left(t_{xn,1} + t_{xn,2} + t_{xn,3}\right)/3 + \left(N_g - t_{R,g}\right) * \left(Rand - 0.5\right) * 2 \quad (10)$$

where $t_{h,g}$ is the i-th tree in the j-th dimension, $t_{xn,1}$, $t_{xn,2}$, and $t_{xn,3}$ represent the first three saved trees before seed generations, $\left(t_{xn,1} + t_{xn,2} + t_{xn,3}\right)/3$ indicates gravity center of the first three trees in the current iteration, N_g implies best tree location in the j-th dimension obtained thus far, and $t_{R,g}$ is a randomly selected tree from the population in the g-th dimension. The working process of feature optimization using IT2SO is summarized in Algorithm 1.

Algorithm 1 Feature optimization using IT2SO

Input: Known features, deep features, maximum iteration, threshold condition	
Output: Feature optimization	
1.	Set up the number of tree population (B)
2.	The initialization of the tree, $t_{h,g} = l_{g,Min} + R_{h,g} \times \left(I_{g,Max} - l_{g,Max}\right)$
3.	Set the problems dimensions (C)
4.	While FEs <Max FEs
5.	The seeds' generation is generated by $s_{h,g} = t_{h,g} + \alpha_{h,g} \times \left(N_g - t_{R,g}\right)$
6	In SCA, the following position updated in both phases: $P_h^{T+1} = P_h^T + R_1 \times \sin(R_2) \times \left\| R_3 X_h^T - P_h^T \right\|, R_4 < 0.5$

7.	If rand <X
8.	Evaluate the objective of the tree (t)
9.	Update the FEs
10.	End if
11.	End for
12.	End while

Axial Flow Fan Design Monitoring and Maintenance

Axial flow fan design monitoring and maintenance involve ensuring the optimal performance and longevity of these fans used in industrial and HVAC systems. They are vital for moving air or gas in a straight-line, commonly used in ventilation, cooling, and industrial processes. The computed optimized features are then input into the deep boosted hybrid learning (DBHL) technique, serving as the decision model for design monitoring and maintenance. DBHL consists of four feature extraction blocks, each employing convolutional layers and ReLU activation to capture spatial correlations and non-linearity. These blocks are followed by average (p^{avg}) and max pooling (p^{Max}), to extract region homogeneity and edge features. This systematic approach exhibits characteristic DBHL feature patterns.

$$P_{m,n} = \sum_{h=1}^{R}\sum_{g=1}^{t} P_{m+h-1,n+g-1} F_{h,g} \tag{11}$$

$$P^{Avg}{}_{m,n} = \frac{1}{z^2}\sum_{h=1}^{z}\sum_{g=1}^{z} P_{m+h-1,n+g-1} \tag{12}$$

$$P^{Avg}{}_{m,n} = Max_{h=1,\ldots z,g=1,\ldots z} P_{m+h-1,n+g-1} \tag{13}$$

$$p = \sum_{c}^{C}\sum_{d}^{C} u_c p_d \tag{14}$$

where, Input channels (p) and filter dimensions (F) are represented as (M×N) and (R×t), respectively, with m and n ranging from 1 to M - R + 1 and N - t + 1. 'w' denotes the window size for average and max-pooling, while 'h' illustrates the number of neurons. This approach leverages DBHL's diverse feature generation, replacing softmax with SVM for enhanced generalization. We propose a DBHL technique incorporating a fine-tuned deep learning model based on SL and an SVM as a strong classifier."

$$\sigma(p) = \frac{E^{p_h}}{\sum_{h=1}^{k} E^{p_K}} \tag{15}$$

$$P_{boosted} = F_d(F_{renet-1}(p) \,\|\, F_{renet-2}(p)) \tag{16}$$

$$c(\lambda H - M) = 0 \tag{17}$$

$$(\lambda H - M)E = 0 \tag{18}$$

where σ is the soft max activation function, k is the number of classes, and x represents the extracted features from the penultimate DBHL layer. In DBHL, the boosted feature space is normalized, and the covariance matrix (M) is computed. Eigenvalues and eigenvectors are then derived from M, and 'c' represents its determinant. The top components, chosen to capture high variance, are selected and fed into SVM.

$$z^S p + n = 0 \tag{19}$$

$$\underset{z,\xi_h}{MinD}\sum_{b}^{B}\varsigma_b + \frac{1}{2}\| z \|^2 \tag{20}$$

The reduced feature space (p) serves as input, while z^S and n represents the weight feature-space orthogonal to the hyper-plane, and bias is the bias term. SVM optimizes a hyper-plane to balance intra and inter-class variation, with ζ indicating misclassified instances, and D governing the trade-off between misclassification and model generalization. Algorithm 2 outlines the axial flow fan design process, including monitoring and maintenance using the DBHL technique."

Algorithm 2 Design of axial flow fan using DBHL technique

	Input: Optimal best features, control measures and total samples
	Output: Axial flow fan design- monitoring and maintenance
1.	Initialize the random population
2.	$P_{m,n} = \sum_{h=1}^{R}\sum_{g=1}^{t} P_{m+h-1,n+g-1}F_{h,g}$
	Define the characteristics patterns
3.	If i=0, j=1
4.	While **Do**
5.	$\sigma(p) = \frac{E^{p_h}}{\sum_{h=1}^{k} E^{p_K}}$
	Compute the boosted feature spaces
6	The reduced feature space (p) is an input instance
7.	If not discard **then**
8.	$\underset{z,\xi_h}{MinD}\sum_{b}^{B}\varsigma_b + \frac{1}{2}\| z \|^2$
	Compute the capture high variance
9.	Find the best output values
10.	End if
11.	End

3. Results and Discussion

In this section, we present the results and compare our design approach, along with monitoring and maintenance processes, with existing methods for axial flow fans. To evaluate the proposed IT2SO+DBHL technique, we use a dataset from the Air Movement and Control Association International (AMCA). We implement the technique in Python via the Anaconda distribution, leveraging libraries such as scikit-learn, Keras, TensorFlow, and DEAP.

Dataset description

AMCA, an international non-profit organization, certifies air-handling equipment like fans, louvers, and dampers [31], offering third-party testing and certification services that benefit global manufacturers, while also contributing to industry standards. We employed the SW-300 fan performance measurement system in this research, illustrated in the wind tunnel equipment diagram. The equipment dimensions are 1.9m x 1.5m x 1.4m, with a DC 60V, 10A, and 600W power supply system. The study involved testing 19 small axial flow fans, measuring pressure, flow rate, and fan speed, while analyzing various fan parameters like chord lengths, pitch angles, and impeller characteristics. The dataset was collected from these 19 fan types and randomly split into three subsets: 70% for training, 15% for validation, and 15% for testing. Data scaling techniques were applied to ensure unbiased model performance analysis.

Quality measure

In this analysis, we evaluate the performance of the proposed IT2SO+DBHL technique alongside established methods using various quality measures, including accuracy, precision, recall, specificity, and F-measure. We compare the results of the IT2SO+DBHL technique with existing methods, including decision tree (DT), random forest (RF), k-nearest neighbor (k-NN), logistic regression (LR), support vector machine (SVM), and deep neural network with genetic algorithm (DNN-GA) [31]. The detailed comparison of the proposed and existing techniques with training samples is discussed in Table 1. The proposed IT2SO+DBHL technique demonstrates a remarkable 22.948% increase in accuracy when compared to DT. Additionally, IT2SO+DBHL surpass DT by approximately 21.948% in precision, 21.948% in recall, 21.948% in specificity, and 21.949% in F-measure. These substantial improvements underscore the superior predictive power of IT2SO+DBHL in low-rate prediction tasks.

In addition to the notable 18.290% increase in accuracy, IT2SO+DBHL show significant improvements over RF. It achieves approximately 20.249% higher precision, 20.231% higher recall, 20.267% higher specificity, and 19.992% higher F-measure compared to RF. These enhancements highlight the robust performance of IT2SO+DBHL. Alongside the significant 14.632% increase in accuracy, IT2SO+DBHL excel in other parameters when compared to k-NN. It achieves approximately 18.632% higher precision, 18.677% higher recall, 18.698% higher specificity, and 18.353% higher F-measure. These improvements emphasize the effectiveness of IT2SO+DBHL in capturing low-rate events. In addition to the substantial 10.974% increase in accuracy, IT2SO+DBHL outperform LR across other parameters. It exhibits approximately 11.974% higher precision, 11.974% higher recall, 11.975% higher specificity, and 11.974% higher F-measure. It highlights IT2SO+DBHL's accuracy and precision in low-rate prediction tasks. IT2SO+DBHL demonstrate an impressive 7.316% increase in accuracy compared to SVM. It also excels in other parameters, achieving approximately 7.315% higher precision, 7.315% higher recall, 7.316% higher specificity, and 7.316% higher F-measure. These improvements underscore the model's capacity to discern low-rate events effectively. These enhancements reinforce IT2SO+DBHL's effectiveness in low-rate prediction tasks, even when compared to robust existing techniques. Form Fig. 2, we summarize that the proposed IT2SO+DBHL technique not only excels in accuracy also shows significant improvements in precision, recall, specificity, and F-measure across all the compared techniques.

Table 1 Quality measure comparison for low-rate prediction

Techniques	Quality measure (%)				
	Accuracy	Precision	Recall	Specificity	F-measure
	Training				
DT	74.921	72.614	73.417	71.620	73.013
RF	78.579	76.272	77.075	75.278	76.671
k-NN	82.237	79.930	80.733	78.936	80.329
LR	85.895	83.588	84.391	82.594	83.988
SVM	89.553	87.246	88.049	86.252	87.646
DNN-GA [31]	93.211	90.904	91.707	89.910	91.304
IT2SO+DBHL	96.869	94.562	95.365	93.568	94.962
	Testing				
DT	63.051	60.941	60.505	59.384	60.722
RF	68.415	66.305	65.869	64.748	66.086
k-NN	73.779	71.669	71.233	70.112	71.450
LR	79.143	77.033	76.597	75.476	76.814
SVM	84.507	82.397	81.961	80.840	82.178
DNN-GA [31]	89.871	87.761	87.325	86.204	87.542
IT2SO+DBHL	95.235	93.125	92.689	91.568	92.906

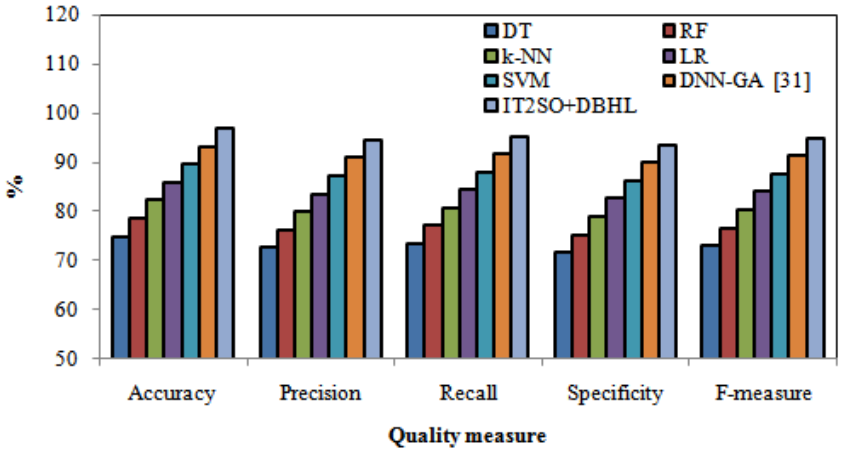

(a)

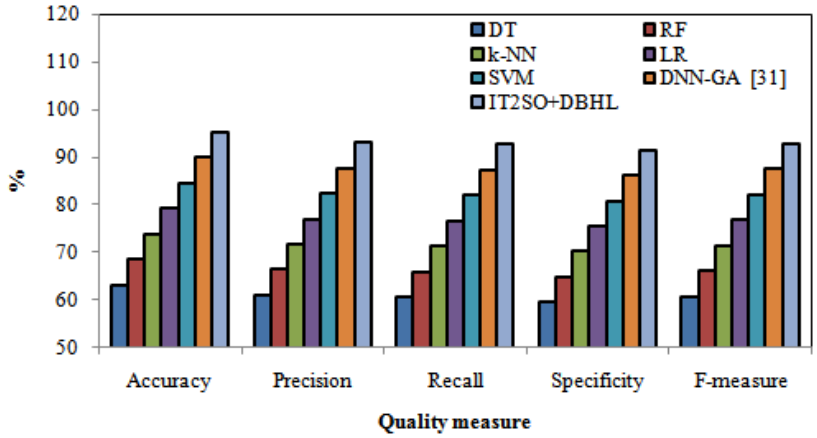

(b)

Fig. 2 Results comparison of quality measure for low-rate prediction with (a) training (b) testing samples

A detailed discussion of the results for low-rate prediction with testing samples discussed in Table 1. In terms of accuracy, DT achieves 63.051%, while the proposed IT2SO+DBHL technique significantly outperforms it by demonstrating an impressive 32.184% increase, reaching an accuracy rate of 95.235%. This substantial gain showcases the robust predictive capabilities of IT2SO+DBHL in low-rate prediction. IT2SO+DBHL excel in precision by approximately 32.184%, recall by around 32.184%, specificity by roughly 32.183%, and F-measure by about 32.184% when compared to DT. RF achieves 68.415% accuracy, and IT2SO+DBHL surpasses it by a remarkable 26.820% increase, attaining an accuracy rate of 95.235%. This substantial improvement underscores the superior predictive power of IT2SO+DBHL in low-rate prediction tasks. IT2SO+DBHL excel in precision by approximately 26.820%, recall by around 26.819%, specificity by roughly 26.819%, and F-measure by about 26.819% when compared to RF. With an accuracy rate of 73.779%, k-NN is significantly surpassed by IT2SO+DBHL, which exhibits an impressive 21.456% increase, achieving an accuracy rate of 95.235%. This substantial gain highlights IT2SO+DBHL's capability to accurately classify low-rate events. IT2SO+DBHL excel in precision by 21.456%, recall by around 21.456%, specificity by roughly 21.455%, and F-measure by about 21.456% when compared to k-NN. LR achieves an accuracy rate of 79.143%, and IT2SO+DBHL outperforms it with a remarkable 20.092% increase, reaching an accuracy rate of 95.235%. IT2SO+DBHL excel in precision by approximately 20.092%, recall by around 20.092%, specificity by roughly 20.091%, and F-measure by about 20.092% when compared to LR. SVM records an accuracy rate of 84.507%, and IT2SO+DBHL surpass it with a notable 10.728% increase, achieving an accuracy rate of 95.235%. This substantial gain underscores IT2SO+DBHL's capacity to accurately classify low-rate events. IT2SO+DBHL excel in precision by approximately 10.728%, recall by around 10.728%, specificity by roughly 10.727%, and F-measure by about 10.728% when compared to SVM. Despite the strong performance of DNN-GA, which achieves 89.871% accuracy, IT2SO+DBHL shows a notable 5.364% increase in accuracy, reaching an accuracy rate of 95.235%. This increase further accentuates IT2SO+DBHL's excellence in low-rate prediction. IT2SO+DBHL excel in precision by 5.364%, recall by around 5.364%, specificity by roughly 5.363%, and F-measure by 5.364% when compared to DNN-GA. Our IT2SO+DBHL technique demonstrates remarkable improvements in accuracy, precision, recall, specificity, and F-measure when compared to each of the existing techniques in Fig. 2.

Table 2 provides a detailed discussion of the results for static pressure prediction with training samples. DT achieves an accuracy of 70.726%, while the proposed IT2SO+DBHL technique demonstrates a remarkable 27.130% increase, reaching an accuracy rate of 97.856%. This substantial gain underscores IT2SO+DBHL's superior predictive capabilities in static pressure prediction. Additionally, IT2SO+DBHL excel in precision by approximately 27.130%, recall by around 27.131%, specificity by roughly 27.130%, and F-measure by about 27.130% when compared to DT. RF records an accuracy rate of 75.248%, and IT2SO+DBHL surpass it with a notable 22.608% increase, achieving an accuracy rate of 97.856%. This significant improvement emphasizes IT2SO+DBHL's effectiveness in static

pressure prediction tasks. IT2SO+DBHL excel in precision by approximately 22.608%, recall by around 22.609%, specificity by roughly 22.608%, and F-measure by about 22.608% when compared to RF. With an accuracy rate of 79.769%, k-NN is significantly surpassed by IT2SO+DBHL, which exhibits an impressive 18.087% increase, achieving an accuracy rate of 97.856%. This substantial gain highlights IT2SO+DBHL's capability to accurately predict static pressure. Furthermore, IT2SO+DBHL excel in precision by approximately 18.087%, recall by around 18.087%, specificity by roughly 18.087%, and F-measure by about 18.087% when compared to k-NN. LR achieves an accuracy rate of 84.291%, and IT2SO+DBHL outperforms it with remarkable 13.565% increase, reaching an accuracy rate of 97.856%.

Table 2 Quality measure comparison for static pressure prediction

Techniques	Quality measure (%)				
	Accuracy	Precision	Recall	Specificity	F-measure
	Training				
DT	70.726	69.328	69.222	68.100	69.275
RF	75.248	73.850	73.744	72.622	73.797
k-NN	79.769	78.371	78.265	77.143	78.318
LR	84.291	82.893	82.787	81.665	82.840
SVM	88.813	87.415	87.309	86.187	87.362
DNN-GA [31]	93.334	91.936	91.830	90.708	91.883
IT2SO+DBHL	97.856	96.458	96.352	95.230	96.405
	Testing				
DT	67.828	65.882	64.126	63.855	64.992
RF	72.350	70.404	68.648	68.377	69.515
k-NN	76.871	74.925	73.169	72.898	74.037
LR	81.393	79.447	77.691	77.420	78.559
SVM	85.915	83.969	82.213	81.942	83.081
DNN-GA [31]	90.436	88.490	86.734	86.463	87.604
IT2SO+DBHL	94.958	93.012	91.256	90.985	92.126

IT2SO+DBHL excel in precision by approximately 13.566%, recall by around 13.566%, specificity by roughly 13.566%, and F-measure by about 13.566% when compared to LR. SVM records an accuracy rate of 88.813%, and IT2SO+DBHL surpass it with a notable 9.043% increase, achieving an accuracy rate of 97.856%. This substantial gain underscores IT2SO+DBHL's capacity to accurately predict static pressure. IT2SO+DBHL excel in precision by approximately 9.043%, recall by around 9.043%, specificity by roughly 9.043%, and F-measure by about 9.043% when compared to SVM. Despite the strong performance of DNN-GA, which achieves 93.334% accuracy, IT2SO+DBHL shows a notable 4.522% increase in accuracy, reaching an accuracy rate of 97.856%. IT2SO+DBHL excel in precision by approximately 4.522%, recall by around 4.522%, specificity by roughly 4.522%, and F-measure by 4.522% when compared to DNN-GA. Our IT2SO+DBHL technique not only excels in accuracy but also demonstrates significant improvements in precision, recall, specificity, and F-measure when compared to each of the existing techniques in Fig. 3.

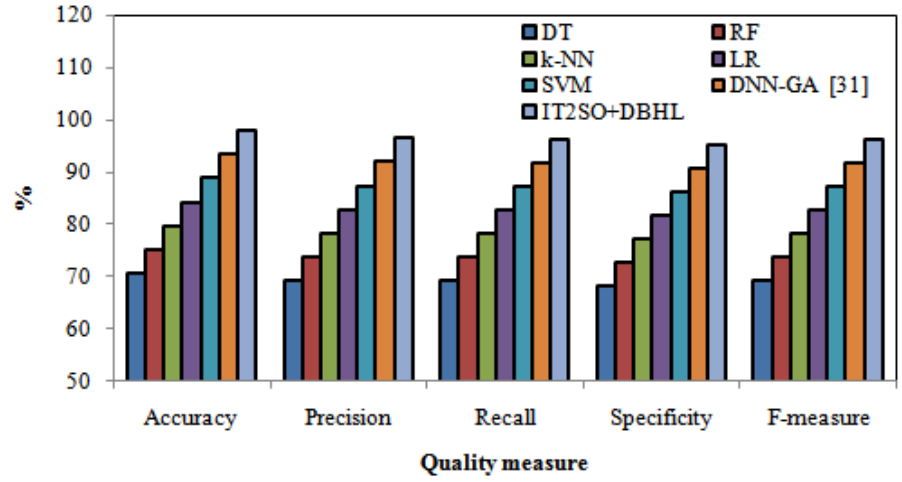

(a)

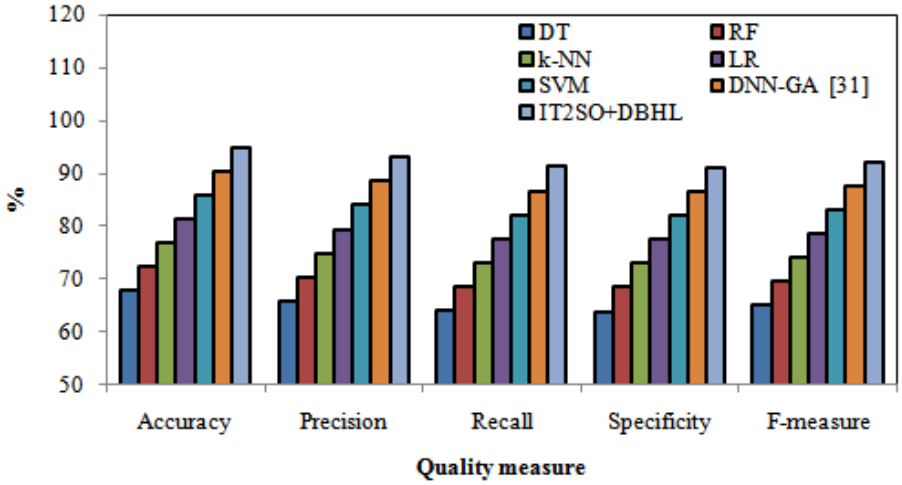

(b)

Fig. 3 Results comparison of quality measure for static pressure prediction with (a) training (b) testing samples

Table 2 provides a detailed discussion of the results for static pressure prediction with testing samples. DT achieves an accuracy of 67.828%, while the proposed IT2SO+DBHL technique significantly outperforms it by demonstrating an impressive 27.130% increase, reaching an accuracy rate of 94.958%. This substantial gain showcases IT2SO+DBHL's superior predictive capabilities in static pressure prediction. IT2SO+DBHL excel in precision by approximately 27.130%, recall by around 27.131%, specificity by roughly 27.130%, and F-measure by about 27.130% when compared to DT. RF records an accuracy rate of 72.350%, and IT2SO+DBHL surpass it with a notable 22.608% increase, achieving an accuracy rate of 94.958%. This significant improvement emphasizes IT2SO+DBHL's effectiveness in static pressure prediction tasks. IT2SO+DBHL excel in precision by approximately 22.608%, recall by around 22.609%, specificity by roughly 22.608%, and F-measure by about 22.608% when compared to RF. With an accuracy rate of 76.871%, k-NN is significantly surpassed by IT2SO+DBHL, which exhibits an impressive 18.087% increase, achieving an accuracy rate of 94.958%. This substantial gain highlights IT2SO+DBHL's capability to accurately predict static pressure. IT2SO+DBHL excel in precision by approximately 18.087%, recall by around 18.087%, specificity by roughly 18.087%, and F-measure by about 18.087% when compared to k-NN. LR achieves an accuracy rate of 81.393%, and IT2SO+DBHL outperforms it with a remarkable 13.565% increase, reaching accuracy rate of 94.958%. This significant improvement emphasizes IT2SO+DBHL's effectiveness in static pressure prediction. IT2SO+DBHL excel in precision by approximately 13.566%, recall by around 13.566%, specificity by roughly 13.566%, and F-measure by about 13.566% when compared to LR. SVM records an accuracy rate of 85.915%, and IT2SO+DBHL

surpass it with a notable 9.043% increase, achieving an accuracy rate of 94.958%. This substantial gain underscores IT2SO+DBHL's capacity to accurately predict static pressure. IT2SO+DBHL excel in precision by approximately 9.043%, recall by around 9.043%, specificity by roughly 9.043%, and F-measure by about 9.043% when compared to SVM. Despite the strong performance of DNN-GA, which achieves 90.436% accuracy, IT2SO+DBHL shows a notable 4.522% increase in accuracy, reaching an accuracy rate of 94.958%. IT2SO+DBHL excel in precision by approximately 4.522%, recall by around 4.522%, specificity by roughly 4.522%, and F-measure by about 4.522% when compared to DNN-GA. Our IT2SO+DBHL technique not only excels in accuracy but also demonstrates significant improvements in precision, recall, specificity, and F-measure when compared to each of the existing techniques in Fig.3.

Error measure

Table 3 provides a detailed discussion of the error measure comparison for both flow rate and static pressure prediction. For flow rate prediction, the R2 value for DNN-GA is 0.9940, while the proposed IT2SO+DBHL technique achieves a significantly higher R2 of 0.9980 in the training phase. In the testing phase, DNN-GA achieves an R2 of 0.9910, and IT2SO+DBHL maintain a superior R2 of 0.9960. These results indicate that IT2SO+DBHL outperform DNN-GA with a substantial increase in R2 in both training and testing, shows its improved predictive accuracy. DNN-GA and IT2SO+DBHL demonstrate remarkably low MAE values of 0.0000 in the training phase. In the testing phase, DNN-GA records a MAE of 0.0010, while IT2SO+DBHL achieves a lower MAE of 0.0009. IT2SO+DBHL exhibits a slight decrease in MAE compared to DNN-GA in the testing phase, signifying its superior accuracy in predicting flow rates. In the training phase for flow rate prediction, DNN-GA and IT2SO+DBHL yield identical RMSE values of 0.0010. However, in the testing phase, DNN-GA produces an RMSE of 0.0010, while IT2SO+DBHL achieve a lower RMSE of 0.0008. This demonstrates that IT2SO+DBHL maintain better accuracy with a reduced RMSE for flow rate prediction.

Table 3 Error measure comparison for both Flow rate and static pressure prediction

Error measure	Training		Testing	
	DNN-GA [31]	IT2SO+DBHL	DNN-GA [31]	IT2SO+DBHL
	Flow rate prediction			
R^2	0.9940	0.9980	0.9910	0.9960
MAE	0.0000	0.0000	0.0010	0.0009
RMSE	0.0010	0.0010	0.0010	0.0008
	Static pressure prediction			
R^2	0.998	0.999	0.997	0.998
MAE	0.420	0.258	0.565	0.326
RMSE	0.613	0.517	0.818	0.587

For static pressure prediction, DNN-GA achieves an R2 of 0.998 in the training phase, while IT2SO+DBHL surpass it with an R2 of 0.999. In the testing phase, DNN-GA records an R2 of 0.997, and IT2SO+DBHL maintain superior R2 of 0.998. IT2SO+DBHL's enhanced predictive capability, with higher R2 values in both training and testing compared to DNN-GA. DNN-GA and IT2SO+DBHL exhibit different MAE values. In the training phase, DNN-GA has a MAE of 0.420, while IT2SO+DBHL achieve a lower MAE of 0.258, indicating superior accuracy for IT2SO+DBHL. In the testing phase, DNN-GA's MAE is 0.565, whereas IT2SO+DBHL maintain a lower MAE of 0.326, demonstrating its improved accuracy in static pressure prediction. In the training phase, DNN-GA records an RMSE of 0.613 while IT2SO+DBHL achieve a lower RMSE of 0.517, indicating its superior accuracy. In the testing phase, DNN-GA produces an RMSE of 0.818, whereas IT2SO+DBHL maintains a lower RMSE of 0.587, further underscoring its enhanced accuracy in static pressure prediction.

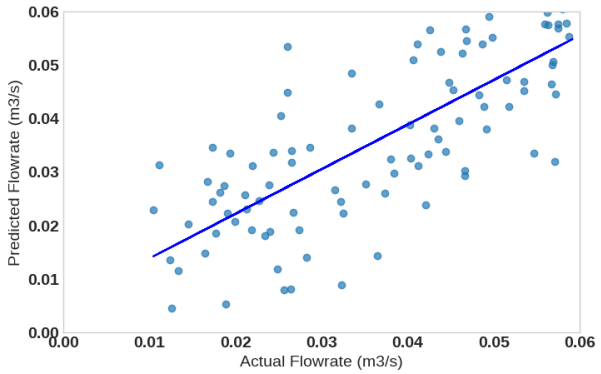

(a)

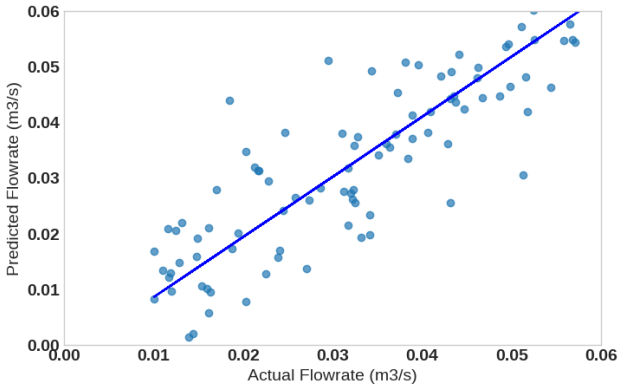

(b)

Fig. 4 Plot of the flow rate prediction using (a) training and (b) testing samples

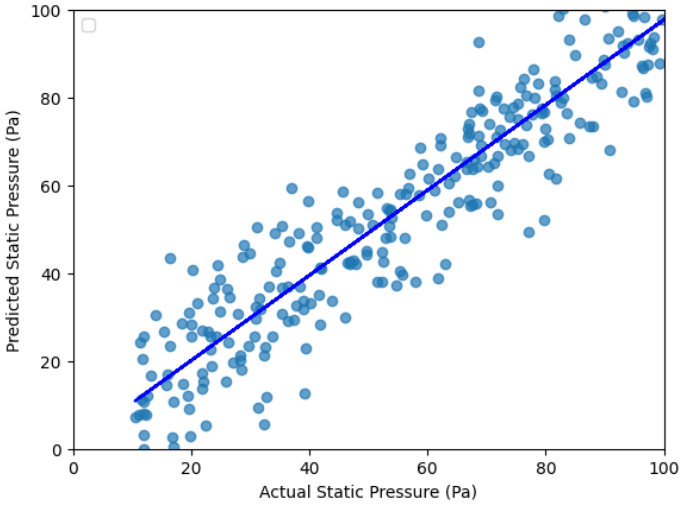

(a)

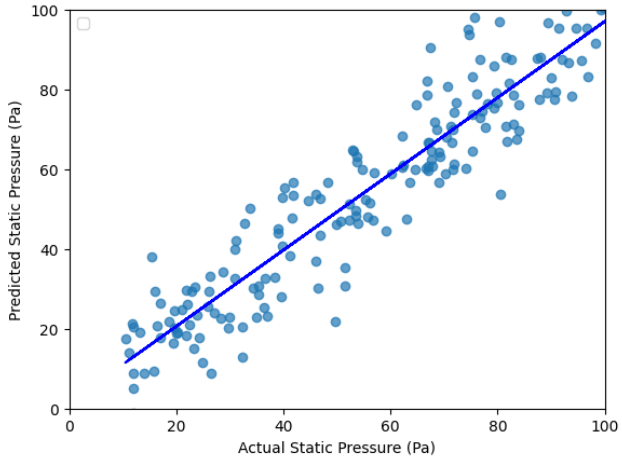

(b)

Fig. 5 Plot of the static pressure prediction using (a) training and (b) testing samples

Fig. 4 illustrates a comparison between the actual and predicted flow rates using both training and testing samples. Meanwhile, Fig. 5 presents a similar comparison but for static pressure prediction using the same training and testing datasets. These two figures collectively serve as visual evidence showcasing the enhanced predictive performance of IT2SO+DBHL in the context of axial flow fan design. The effectiveness of the proposed IT2SO+DBHL methodology in improving the accuracy of predicting these crucial parameters is clearly demonstrated through these graphical representations.

4. Conclusion

Our approach introduces a novel method for monitoring and maintaining axial flow fans through the integration of optimal deep learning with an IoT system. We employ the pre-trained U-Net architecture to effectively extract concealed features from the dataset. Additionally, we introduce the improved triple tree-seed optimization (IT2SO) algorithm, which plays a crucial role in optimizing the extracted features, allowing us to identify the most relevant ones. To support informed decision-making for the monitoring and maintenance of axial flow fans, we propose the utilization of the deep boosted hybrid learning (DBHL) technique as the decision model to ensure their proper operation. To validate the effectiveness of our IT2SO+DBHL approach, we conducted rigorous experiments using the air movement and control association international (AMCA) dataset. The outcomes of these experiments unequivocally demonstrate the superior performance of our monitoring and maintenance methodology when compared to existing techniques. This superiority is evident in terms of both quality measures and error assessments, underlining the substantial advancements our approach brings to the field of axial flow fan management.

References:

1. Vansompel, H., Rasekh, A., Hemeida, A., Vierendeels, J. and Sergeant, P., 2015. Coupled electromagnetic and thermal analysis of an axial flux PM machine. IEEE Transactions on Magnetics, 51(11), pp.1-4.
2. Wu, S.T., Huang, P.W., Chang, T.W., Jiang, I.H. and Tsai, M.C., 2020. Application of magnetic metal 3-D printing on the integration of axial-flow impeller fan motor design. IEEE Transactions on Magnetics, 57(2), pp.1-5.
3. Xu, C., Mao, Y. and Hu, Z., 2017. Tonal and broadband noise control of an axial-flow fan with metal foams: Design and experimental validation. Applied Acoustics, 127, pp.346-353.
4. Jung, J.H. and Joo, W.G., 2018. Effect of tip clearance, winglets, and shroud height on the tip leakage in axial flow fans. International Journal of Refrigeration, 93, pp.195-204.
5. Wang, C., 2018. Noise source analysis for two identical small axial-flow fans in series under operating condition. Applied Acoustics, 129, pp.13-26.
6. Zhu, T., Lallier-Daniels, D., Sanjosé, M., Moreau, S. and Carolus, T., 2018. Rotating coherent flow structures as a source for narrowband tip clearance noise from axial fans. Journal of Sound and Vibration, 417, pp.198-215.
7. Chen, L., Yang, L., Du, X. and Yang, Y., 2018. Novel air-cooled condenser with V-frame cells and induced axial flow fans. International Journal of Heat and Mass Transfer, 117, pp.167-182.

8. Ravelet, F., Bakir, F., Sarraf, C. and Wang, J., 2018. Experimental investigation on the effect of load distribution on the performances of a counter-rotating axial-flow fan. Experimental Thermal and Fluid Science, 96, pp.101-110.
9. Ye, X., Ding, X., Zhang, J. and Li, C., 2017. Numerical simulation of pressure pulsation and transient flow field in an axial flow fan. Energy, 129, pp.185-200.
10. Tóth, B. and Vad, J., 2017. Algorithmic localisation of noise sources in the tip region of a low-speed axial flow fan. Journal of Sound and Vibration, 393, pp.425-441.
11. Ye, X., Zhang, J. and Li, C., 2017. Effect of blade tip pattern on performance of a twin-stage variable-pitch axial fan. Energy, 126, pp.535-563.
12. Zanon, A., De Gennaro, M., Kuehnelt, H. and Giannattasio, P., 2018. Assessment of the broadband noise from an unducted axial fan including the effect of the inflow turbulence. Journal of Sound and Vibration, 429, pp.18-33.
13. Canepa, E., Cattanei, A., Zecchin, F.M. and Parodi, D., 2019. Large-scale unsteady flow structures in the leakage flow of a low-speed axial fan with rotating shroud. Experimental Thermal and Fluid Science, 102, pp.1-19.
14. Park, K., Choi, H., Choi, S. and Sa, Y., 2019. Effect of a casing fence on the tip-leakage flow of an axial flow fan. International Journal of Heat and Fluid Flow, 77, pp.157-170.
15. Canepa, E., Cattanei, A. and Zecchin, F.M., 2016. Analysis of tonal noise generating mechanisms in low-speed axial-flow fans. Journal of Thermal Science, 25, pp.302-311.
16. Lim, T.G., Jeon, W.H. and Minorikawa, G., 2016. Characteristics of unsteady flow field and flow-induced noise for an axial cooling fan used in a rack mount server computer. Journal of Mechanical Science and Technology, 30, pp.4601-4607.
17. Chen, X., Cao, L., Yan, P., Wu, P. and Wu, D., 2017. Effect of meridional shape on performance of axial-flow fan. Journal of Mechanical Science and Technology, 31, pp.5141-5151.
18. Song, P. and Sun, J., 2015. Blade shape optimization for transonic axial flow fan. Journal of Mechanical Science and Technology, 29, pp.931-938.
19. Liu, Y., Lin, Z., Lin, P., Jin, Y., Setoguchi, T. and Kim, H.D., 2017. Effect of inlet guide vanes on the performance of small axial flow fan. Journal of Thermal Science, 26, pp.504-513.
20. Spasić, Ž., Jovanović, M. and Bogdanović-Jovanović, J., 2018. Design and performance of low-pressure reversible axial fan with doubly curved profiles of blades. Journal of Mechanical Science and Technology, 32, pp.3707-3712.
21. Mesalhy, O., Rath, C., Rini, D., Kizito, J., Leland, Q. and Chow, L., 2020. A parametric fin structure design study for cooling aerospace electro-mechanical actuators with high-speed axial fans. Heat and Mass Transfer, 56, pp.1565-1577.
22. Angelini, G., Corsini, A., Delibra, G. and Tieghi, L., 2019. Exploration of Axial Fan Design Space with Data-Driven Approach. International Journal of Turbomachinery, Propulsion and Power, 4(2), p.11.
23. Li, J., Chen, H., Liu, Y., Wang, J. and Yang, X., 2019. Aerodynamic design and optimization of a high-loaded axial fan stage using a curvature control method. Journal of Mechanical Science and Technology, 33, pp.3871-3883.
24. Shahsavari, A. and Nili-Ahmadabadi, M., 2020. A novel approach for the design of axial flow fan by increasing by-pass ratio in a constant-diameter turbofan. Propulsion and Power Research, 9(2), pp.142-158.
25. Gu, Z.Y., Zhu, Y.Y., Xiang, J.L. and Zeng, Y., 2021. A prediction method of operation trend for large axial-flow fan based on vibration-electric information fusion. Journal of Central South University, 28(6), pp.1786-1796.
26. Kumar, A., Manas, M.P. and Pradeep, A.M., 2022. Identification and classification of operating flow regimes and prediction of stall in a contra-rotating axial fan using machine learning. The Aeronautical Journal, 126(1302), pp.1351-1369.
27. Ciaburro, G., Padmanabhan, S., Maleh, Y. and Puyana-Romero, V., 2023, February. Fan Fault Diagnosis Using Acoustic Emission and Deep Learning Methods. In Informatics (Vol. 10, No. 1, p. 24). MDPI.
28. Liang, Z., Wang, J., Wang, W., Jiang, B., Ding, Y. and Qin, W., 2023. Numerical and Experimental Investigations of Axial Flow Fan with Bionic Forked Trailing Edge. Machines, 11(2), p.155.
29. Ding, Y., Wang, J., Jiang, B., Li, Z., Xiao, Q., Wu, L. and Xie, B., 2022. Multi-objective optimization for the radial bending and twisting law of axial fan blades. Processes, 10(4), p.753.
30. Chen, F., Zhu, G., Xi, D. and Miao, B., 2023. Air volume flow rate optimization of the guide vanes in an axial flow fan based on DOE and CFD. Scientific Reports, 13(1), p.4439.
31. Liu, Y.L., Nisa, E.C., Kuan, Y.D., Luo, W.J. and Feng, C.C., 2023. Combining deep neural network with genetic algorithm for axial flow fan design and development. Processes, 11(1), p.122.
32. Kiran, M.S., 2015. TSA: Tree-seed algorithm for continuous optimization. Expert Systems with Applications, 42(19), pp.6686-6698